American Mineralogist, Volume 86, pages 411–423, 2001

In situ atomic force microscopy study of hectorite and nontronite dissolution: Implications for phyllosilicate edge surface structures and dissolution mechanisms

BARRY R. BICKMORE,[1,*] DIRK BOSBACH,[2] MICHAEL F. HOCHELLA JR.,[1] LAURENT CHARLET,[3] AND ERIC RUFE[1]

[1]Department of Geological Sciences, 4044 Derring Hall, Virginia Polytechnic Institute and State University, Blacksburg, Virginia 24061, U.S.A.
[2]Institut für Mineralogie, Universität Münster, Corrensstrasse 24, 48149 Münster, Germany
[3]Environmental Geochemistry Group, L.G.I.T., B.P. 53, F-38041 Grenoble Cedex 9, France

ABSTRACT

The dissolution behavior of two smectite minerals, hectorite (trioctahedral) and nontronite (dioctahedral), was observed in situ, in acid solutions, using atomic force microscopy. As expected, the crystallites dissolved inward from the edges, and the basal surfaces appeared to be unreactive during the timescale of the experiments. The hectorite (010) faces appeared to dissolve about 6× more slowly than the lath ends, usually broken edges. The edges visibly dissolved on all sides, and appeared to roughen somewhat. On the other hand, the (010), (110), and (1$\bar{1}$0) faces on nontronite crystals were exceptionally stable, so that any dissolution fronts originating at broken edges or defects would quickly become pinned along these faces, after which no more dissolution was observable. These observations can be explained by using periodic bond chain theory to predict the topology of the surface functional groups on the edge faces of these minerals. If a certain amount of predicted surface relaxation is allowed on the (110) and (1$\bar{1}$0) faces of nontronite, an important difference between the exceptionally stable faces and the others becomes apparent. That is, the oxygen sites connecting the octahedral and tetrahedral sheets are all fully bonded on the nontronite (010), (110), and (1$\bar{1}$0) edge faces, whereas all hectorite edge faces and nontronite broken edges would have coordinatively unsaturated connecting O atoms. This explanation for the differential reactivity of these crystal faces implies that the rate limiting step of the dissolution process is the breaking of bonds to connecting O atoms.

INTRODUCTION

Atomic Force Microscopy (AFM) is a powerful tool to explore various aspects of the structure, microtopography, and surface reactivity of minerals (see Nagy and Blum 1994; Hochella 1995; Hochella et al. 1998). Perhaps its greatest strength, from a geochemical perspective, has been the ability to make quantitative measurements of changing surface microtopography in situ, as minerals react in aqueous solutions (Drake et al. 1989; Hillner et al. 1992; Dove and Hochella 1993; Bosbach and Rammensee 1994; Dove and Chermak 1994; Junta and Hochella 1994; Bosbach et al. 1995; Putnis et al. 1995; Bosbach and Hochella 1996; Bosbach et al. 1996, 1998; Grantham and Dove 1996; Liang et al. 1996; Junta-Rosso et al. 1997; Teng et al. 1998; Rufe and Hochella 1999). Such observations often reveal that some mineral faces are more reactive than others, and given a model of the crystallographic structure of these faces, one can sometimes infer the dominant mechanism(s) of the surface reaction in question (e.g., Liang et al. 1996; Bosbach et al. 1998; Rufe and Hochella 1999).

Due to the extreme anisotropy of their structures, phyllosilicate surfaces have been shown to exhibit strong differential reactivity (Schofield and Samson 1953; White and Zelazny 1988; Anderson and Sposito 1991; Zachara and McKinley 1993; Bleam 1993; Turpault and Trotignon 1994; Brady et al. 1996). However, until recently the applicability of in situ AFM techniques to phyllosilicate surface reactivity has been limited due to two major factors. First, phyllosilicates are generally characterized by only one cleavage plane, i.e., the perfect cleavage along the (001) basal surface. Whereas other faces often occur as preferred growth surfaces, in the case of macroscopic phyllosilicate crystals (e.g., micas) these are usually too narrow or rough for AFM analysis. Zones of mechanical weakness within micas run parallel to the preferred growth faces (Bloss et al. 1959; Klein and Hurlbut 1993), but the small-scale step features generated by cleaving these minerals are generally not euhedral, and hence the "edge" faces available for examination by AFM are randomly oriented surfaces. This makes possible the comparison of the reactivity of non-spe-

* Present address: Department of Geological Sciences, University of Colorado at Boulder, Campus Box 399, Boulder, CO 80309-0399. E-mail: bickmore@colorado.edu

cific edge surfaces with that of the basal planes, but because the structures of the randomly oriented surfaces are not strictly crystallographically constrained, specific mechanistic information is more difficult to infer. Rufe and Hochella (1999) recently overcame this problem to some extent by pre-etching phlogopite surfaces with HF, in order to examine the dissolution behavior of etch pits in HCl and deionized H_2O with in situ AFM. The etch pits were essentially euhedral along the preferred growth faces, and similar features have been generated on various mica surfaces by etching with either HF or fused alkalis (Brauer 1971; Pandya and Pandya 1959; Patel and Ramanathan 1962). Second, although clay minerals (phyllosilicates with a Stokes settling diameter of <2 mm) often exhibit euhedral growth faces at their edges, small enough to examine with AFM, it has been difficult to immobilize such tiny particles on a suitable substrate for in situ analysis (Dove and Chermak 1994). However, Bickmore et al. (1999a) recently described methods for the immobilization of clay minerals for in situ AFM analysis under various solution conditions, and Bosbach et al. (2000) have applied one of these techniques to examine the dissolution behavior of single crystallites of hectorite clay in HCl.

This paper compares the results of Bosbach et al. (2000) on hectorite dissolution with the in situ AFM nontronite dissolution results of this study. We relate the observed differential reactivity of the crystal faces to models of the surface atomic structure of phyllosilicate edge faces, and determine which one best explains our data. Within the framework of the chosen model of the edge surface structure, we then relate our results to current models of the proton-promoted dissolution of phyllosilicates, and determine which one best accounts for the data obtained in this and other studies.

The structure and reactivity of phyllosilicate surfaces is fundamentally important for understanding of ion mobility in the near-surface environment, permeability reduction in reservoir rocks, and many other geochemical processes (e.g., Sposito 1984; Eslinger and Pevear 1988). In situ AFM imaging of reactions on phyllosilicate surfaces makes it possible to acquire information about these topics that would, at best, be very difficult to obtain via other experimental methods now available.

MATERIALS AND METHODS

Samples

Hectorite. Hectorite (SHCa-1, Hector, California) was obtained from the Clay Minerals Society Source Clay Repository. Hectorite $Na_{0.80}(Mg_{5.30}Li_{0.70})(Si_{7.90}Al_{0.10})O_{20}(OH)_4$ (Schlegel et al. 1999) is a trioctahedral, magnesian smectite with some Li substituting for Mg in the octahedral layer. The <2 μm fraction of the sample material was collected, sodium saturated, acid washed, and treated with dithionate-citrate-bicarbonate and H_2O_2 solutions. A more complete description of the preparation and characterization procedures is in Schlegel et al. (1999).

The hectorite crystallites are predominantly lath-shaped, the long edges representing (010) faces, and the shorter edges representing (110), $(1\bar{1}0)$, (100) faces, or broken edges (Oberlin and Méring 1966; Güven 1988; Bosbach et al. 2000).

Nontronite. Nontronite was obtained from Ward's (no. 33A, Garfield, Washington). Garfield nontronite $Na_{0.96}(Fe^{3+}_{3.96}Mg_{0.02}Ti_{0.02})(Si_{6.94}Al_{1.06})O_{20}(OH)_4$ (Bonnin et al. 1985) is a dioctahedral smectite with the montmorillonite structure (Eggleton 1977; Besson et al. 1982, 1983; Bonnin et al. 1985; Manceau et al. 1998). The sample was crushed in a mortar and pestle, suspended in 500 mL of deionized H_2O, and blended in a Waring heavy-duty blender for several minutes. Large fragments were allowed to settle out of the suspension, and the supernatant was decanted. The <2 μm fraction of the suspension was separated by centrifugation. To remove associated Fe oxides (predominantly goethite, see Güven 1991; Murad 1987), the <2 μm fraction was carefully subjected to several sedimentation cycles in deionized H_2O (Manceau et al. 1998). The sample was then acid washed 4 times by shaking for one hour in pH 3.0 HCl, and centrifuging. It was then Na-saturated. Approximately 280 mg of the purified sample was mounted on a ceramic tile for powder X-ray diffraction analysis (Rich 1969), and no secondary phases were detected.

The Garfield nontronite crystallites are predominantly lath-shaped (Güven 1991), the long edges representing (010) faces (Grim and Güven 1978; Güven 1991), and the short edges representing (110), $(1\bar{1}0)$ (White and Zelazny 1988), (100), or broken edge faces.

Clay immobilization

The clays were immobilized for in situ AFM analysis using variations on one of the techniques described by Bickmore et al. (1999a). The exact procedure used for the hectorite sample is described by Bosbach et al. (2000). With the nontronite sample, polyethyleneimine $(C_2H_5N)_n$ (M.W. 1800, Polysciences, Warrington, Pennsylvania) was diluted 1:500 by volume. A small disk of freshly cleaved muscovite was taped with double-sided tape to a similarly shaped steel AFM sample puck and immersed in the suspension for ~30 s. The muscovite was then rinsed with a stream of deionized water for 5 min and dried in a 90 °C oven for 20 min. A dilute suspension of the clay in deionized H_2O (~0.2 mg clay per 20 mL) was prepared and then dispersed for 1–2 min with an Artek sonic dismembrator (Dynatech Laboratories, Chantilly, Virginia, model 300) set at ~150 Watts. The dried PEI-coated muscovite was immersed in the clay suspension for 1 min, and then blown dry with a stream of compressed air.

AFM imaging

Imaging of both the hectorite and nontronite crystallites was performed in the fluid cell of a MultiMode atomic force microscope (Digital Instruments, Santa Barbara, California). Hectorite imaging was performed with pyramidal Si_3N_4 tips, whereas nontronite imaging was performed with oxide-sharpened Si_3N_4 tips. Bosbach et al. (2000) reported that force–distance curves showed a large attractive peak due to the presence of the PEI coating, whereas on clean mica surfaces in aqueous solution there were not such strong adhesive interactions with the AFM tip. This sometimes made it difficult to collect stable images in TappingMode (TMAFM), so contact mode was exclusively used to observe the hectorite dissolution reactions. The strong attraction between the AFM tip and the PEI-coated mica substrate resulted in a tip loading force of about 50–100 nN, and therefore some hectorite particles were stripped from the surface during the course of the experiments. Tip-sample

interaction can result in enhanced dissolution rates of monolayer steps (Park et al. 1996), but Bosbach et al. (2000) reported that they could detect no relationship between scan speed or AFM feedback control parameters and particle edge dissolution rates. We have performed some nontronite dissolution experiments in TMAFM, which results in a much weaker tip-sample interaction (Hansma et al. 1994; Johnson 1995), and some in contact-mode. However, we found that contact-mode imaging did, in fact, enhance the nontronite dissolution rate in a very specific manner, which will be discussed below.

Bosbach et al. (2000) imaged the hectorite under deionized water, and then pH = 2.0 HCl was injected into the cell, after which dissolution was observed. The same procedure was used with the nontronite, although pH = 1.5–2.0 HCl solutions were used.

The AFM images are constructed from height data, and were subjected to the flattening routine (a least-squares polynomial fit to remove unwanted features from the scan lines) included with the Digital Instruments software. We applied 5–10 repetitions of a 3x3 median filter to the images to remove random noise (Russ 1995). Features in the images were analyzed using the Image SXM image analysis program (Barrett 1997).

Crystal structure modeling

The crystal structures and surface planes of hectorite and nontronite were modeled using the program *CrystalMaker* (Palmer 1998; cf. Koretsky et al. 1998). Data used to generate models of the nontronite structure were taken from Besson et al. (1983) and Bonnin et al. (1985). The unit-cell parameters (assuming a single-layer monoclinic unit cell) used to calculate site densities for nontronite are a = 5.28 Å, b = 9.14 Å, c = 10.1 Å, and b = 99°. Atomic coordinates for hectorite were obtained from Oberlin and Méring (1966), as were the a and b parameters. The b angle was estimated at 99°, in agreement with the discussion of smectite minerals in Deer et al. (1992). Given the above, the c cell parameter was adjusted to produce a d_{001} spacing of 9.65 Å, as measured for dehydrated Na-hectorite by Kadi-Hanifi and Méring (1972). Thus, the unit-cell parameters chosen for hectorite are a = 5.25 Å, b = 9.09 Å, c = 9.77 Å, and b = 99°.

The site densities on the (010), (110), and $(1\bar{1}0)$ faces of hectorite and nontronite were calculated by counting the number of sites per planar cell for the (*hkl*) in question. The planar cell areas were calculated by taking the cross product of the vectors defining the parallelogram which outlines a planar cell on that face (Boisen and Gibbs 1985). Given the above, the unit-cell face areas for nontronite are $A_{(010)}$ = 0.527 nm^2, and $A_{(110)} = A_{(1\bar{1}0)}$ = 1.063 nm^2, and the unit-cell face areas for hectorite are $A_{(010)}$ = 0.507 nm^2, and $A_{(110)} = A_{(1\bar{1}0)}$ = 1.080 nm^2.

Results and discussion

Differential reactivity of crystal faces

Hectorite dissolution. Bosbach et al. (2000) report that the dissolution of the hectorite laths appeared to occur exclusively at the edge surfaces during the time scale of the experiments (up to several hours). A continuous decrease in particle volume occurred. The particle length to width ratio did not change significantly during the dissolution process, which, given the morphology of the crystallites, suggested that the average dissolution rate at the ends of the laths (usually broken edges) was about 6 times faster than at the lath sides, which were generally euhedral (010) faces. Even euhedral edges of the laths appeared to "roughen" slightly over time (see Fig. 1). The basal (001) surfaces did not appear to participate in the reaction.

Nontronite dissolution. The nontronite also appeared to dissolve exclusively from the edges during the time scale of these experiments (up to 5 hours). Particle heights for several flat laths were measured over time during contact mode dissolution experiments using smoothed height histograms of the area of the image around each particle (Bickmore et al. 1999b), and it was found that the particle height did not significantly change over time for several very flat nontronite laths observed in various dissolution experiments (Fig. 2). Significant disso-

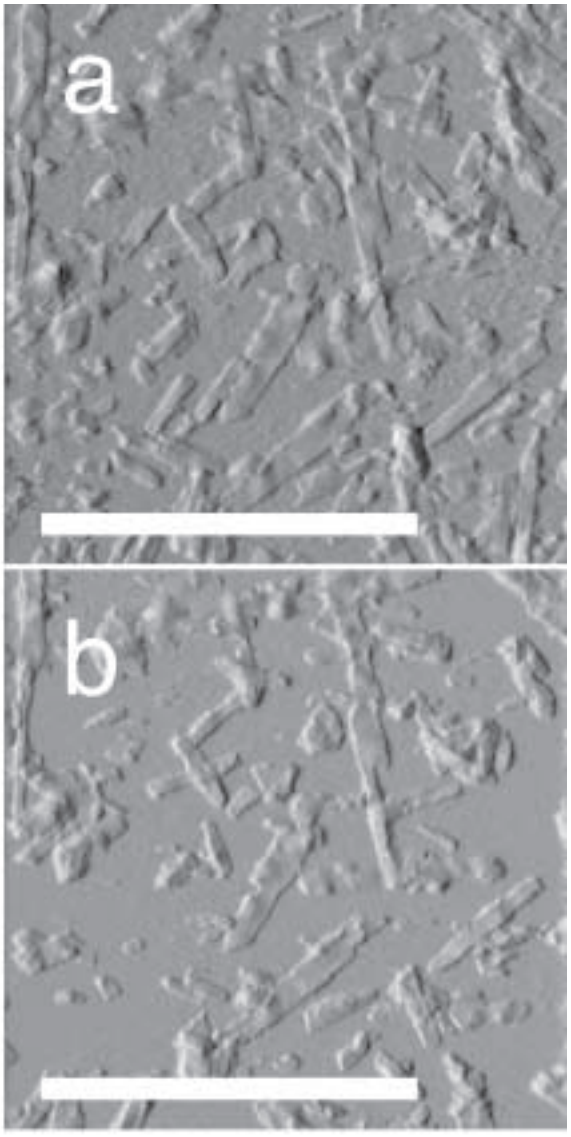

Figure 1. AFM deflection images of hectorite laths during a dissolution experiment. (**a**) Under deionized water. (**b**) The same area after 45 min exposure to pH 2 HCl. Scale bar = 1 μm. Most particles are ~2 nm in height.

lution of all these particles was observed at the edge surfaces, but the particle heights did not change appreciably over time except for the two tallest particles in the plot, off of which approximately 5 Å of detrital material was immediately cleared, and then no further height change was observed. Similarly, no etch pits were observed to form on the basal surfaces of the laths. The average measured particle heights for the laths analyzed for Figure 2 generally were 3.3–3.5 nm, and one was ~1.7 nm. In contact mode, the AFM tip appears to scrape aside the PEI coating from the mica substrate surface. Therefore, these values are consistent with 2 or 1 unit-cell high particles, respectively, because the height of one T-O-T layer (0.9–1 nm) plus the height of a monolayer of PEI (0.6 ± 0.3 nm) (Bickmore et al. 1999a; Bosbach et al. 2000) would be approximately 1.2–1.9 nm, and the added height of another T-O-T layer plus a Na-saturated interlayer (0.5–1 nm) would result in a particle height of 2.7–3.9 nm.

Very little dissolution even at the edge surfaces of the nontronite laths was observed in TMAFM, except where ragged edges seemed to straighten somewhat so that the edges more exactly paralleled the euhedral edge faces.

In contact mode, however, the dissolution at the edge surfaces was enhanced in two ways. First, due to the large tip-sample attraction, long, thin portions of the laths were sometimes broken off by the AFM tip, creating a high-energy, randomly oriented surface. Second, the tip sometimes appeared to "nick" the edges of the particles, again creating a high-energy, randomly oriented defect surface. Both the broken edges and the defect sites dissolved very quickly, until the dissolution front became pinned parallel to the (010), (110), and ($1\bar{1}0$) faces. In rare cases what appeared to be (100) surfaces were observed at the ends of nontronite laths, which sometimes appeared to be stable under acid conditions, but the reaction fronts established at other broken edges and defect sites were never observed to stabilize along the (100) plane. This behavior is illustrated in a time series of AFM images taken during the dissolution of several nontronite crystallites in pH 2.0 HCl (Fig. 3). The dissolution behavior of the two laths near the center of the

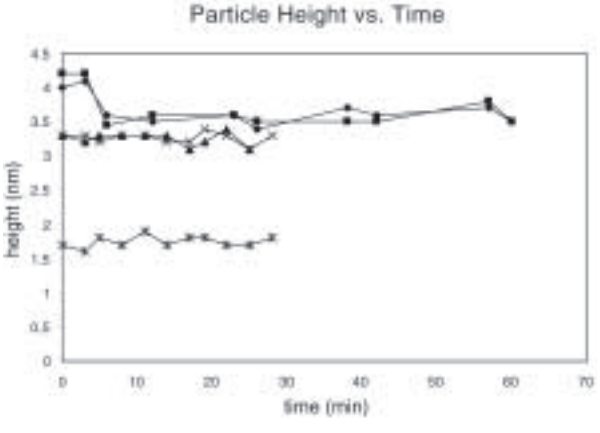

FIGURE 2. Measured particle heights of several very flat nontronite laths over time during dissolution experiments. Whereas significant dissolution took place at the edges of all these particles, the particle heights appeared to stay essentially constant.

images is especially relevant. Figure 3a was taken under deionized water, whereas Figure 3b was taken just 6 min after injection of the acid. At 6 min exposure, the outline of the laths appear to have "sharpened" along the (010), (110), and ($1\bar{1}0$) faces. At 38 min exposure (Fig. 3c), the probe tip appears to have nicked the top lath at point A, and the dissolution front has retreated to the point where it has started to approximate the euhedral face angles. Similarly, the tip appears to have nicked the bottom lath at point B, and the dissolution front there has proceeded inward and then been pinned along the euhedral face planes. After 60 min exposure (Fig. 3d), the outline of the top lath appears to have remained fairly stable, whereas the probe tip appears to have broken off the end of the bottom lath at point C, and nicked it at point D, after which the dissolution fronts in these areas proceeded inward until they again became pinned parallel to the directions of the euhedral faces.

Edge vs. basal surface reactivity. The basal surfaces of neither the hectorite nor the nontronite particles appeared to significantly participate in the dissolution reactions within the time scale of these experiments (up to several hours). This is to be expected, because the basal surfaces are characterized exclusively by charge-satisfied and extremely stable siloxane bonds, whereas the edge surfaces are characterized by broken bonds and a well-known tendency to form inner-sphere complexes with protons and other cations (e.g., White and Zelazny 1988; Zachara and McKinley 1993; Charlet et al. 1993; Schlegel et al. 1999). Similarly, Turpault and Trotignon (1994) dissolved macroscopic flakes of biotite of known dimensions in pH 1.08 HNO_3 at 24 °C, and demonstrated that the edge surfaces were approximately 250 times more reactive than the basal surfaces. In addition, Rufe and Hochella (1999) performed in situ TMAFM acid dissolution experiments on pre-etched phlogopite surfaces, and found that the dissolution reaction in its early stages occurs via retreat of monolayer edge steps whereas basal surfaces remain stable. Based on ^{19}F MAS NMR data, Kaviratna and Pinnavaia (1994) inferred that the acid hydrolysis of fluorohectorite proceeded almost exclusively at the edge surfaces, and only in its late stages at the basal surfaces. Because our experiments lasted no more than several hours, our data are consistent with these studies, and also with the general consensus over several decades that the acid hydrolysis of 2:1 phyllosilicates essentially proceeds exclusively at the edge surfaces through most of the reaction (see Nagy 1995, and references therein).

Hectorite vs. nontronite edge surface reactivity. The difference in reactivity between the hectorite and nontronite edge faces is very interesting. Whereas the nontronite edge surfaces appeared to straighten, to more closely parallel the euhedral face planes, the hectorite edge surfaces roughened over time. Whereas the nontronite edge surfaces dissolved much faster at broken edges and defect sites (whether tip-induced or not), and the reaction fronts eventually became pinned at the euhedral face plane angles, the hectorite edge surfaces all appeared to dissolve at relatively similar rates.

These observations indicate first that the active sites at the hectorite edge surfaces are all similar in their reactivity. Whereas broken edges may have some especially reactive sites, which

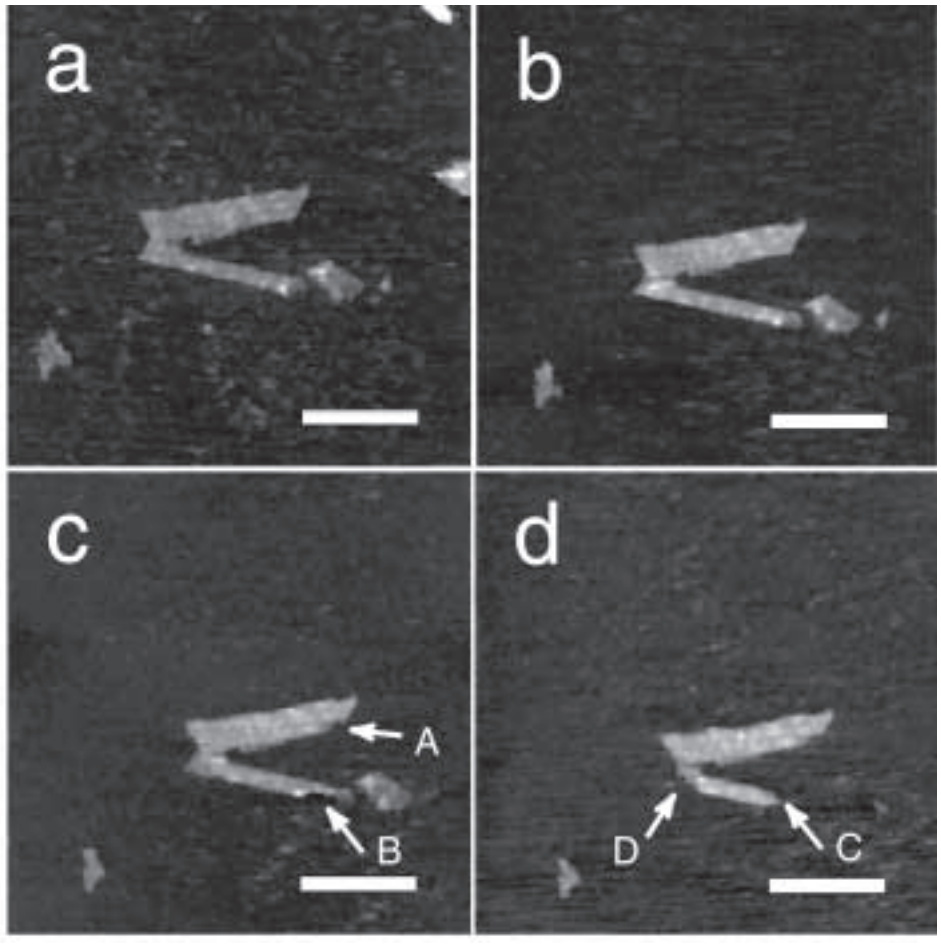

FIGURE 3. AFM height images of nontronite laths after (**a**) 0 min, (**b**) 6 min, (**c**) 38 min, and (**d**) 60 min of exposure to pH 2 HCl. Scale bar = 1 μm. The two particles in the middle are both ~4 nm in height.

enhance their step retreat rate somewhat, the reactivity of the euhedral edge faces was comparable. The fact that the euhedral edge surfaces appeared to roughen over time graphically illustrates that their reactivity is similar to non-euhedral faces. These obserations also indicate that active sites at the nontronite euhedral edge faces are much, much less reactive than those at broken edges and defects. It was pointed out that the AFM tip appeared to generate defect sites at the edges, which greatly enhanced their reactivity. In contrast, such defects were undoubtedly generated during the experiments on the hectorite laths, but a similar increase in reactivity was not observed.

Implications for edge surface structure

Models of phyllosilicate edge surface structures. These conclusions about the reactivity of hectorite and nontronite edge surfaces obviously must be explained in terms of their atomic structure and reactivity. However, given the morphology and chemistry of these minerals, it is not presently possible to directly probe the structure of specific phyllosilicate edge surfaces using techniques like low energy electron diffraction or scanning tunneling microscopy (see Hochella 1990). To date models of phyllosilicate edge surface structure have usually been derived using established crystallochemical principles (see Bleam 1993).

Schematic models of the types of sites available at phyllosilicate edge surfaces have been proposed to explain their observed pH dependent charge (Schofield and Samson 1953; Muljadi et al. 1966; van Santen 1982). More detailed and useful models have been constructed, taking into account differences in the crystal structure parallel to preferred growth faces. White and Zelazny (1988) used the crystal growth theory (or, more precisely, the crystal morphology theory) of Hartman and Perdock (1955a, 1955b, 1955c; Hartman 1963, 1973, 1978; cf. Paquette and Reeder 1990; Fouke and Reeder 1992) to predict the topology of surface sites on the (110), ($1\bar{1}0$), and (010) faces of dioctahedral phyllosilicates. They further speculated that a certain amount of bond relaxation occurred on the (110) and ($1\bar{1}0$) faces, leaving them uncharged at normal pH levels (pH 3–9). Bleam et al. (1993) used an identical method to predict the topology of the same surfaces on pyrophyllite, as well as the (100) and (130) faces. However, they did not allow for surface relaxation, but instead used an unrelaxed surface configuration, and optimized the surface OH bond vectors to obtain the surface Coulomb energy and proton Coulomb energy for these faces. Koretsky et al. (1998) predicted the site types and densities on prominent crystal faces of several minerals, including the kaolinite (010) and (110) faces, by slicing the crystal structures along planes that produced the minimum total

strength of bonds severed, calculated using the method of Altermatt and Brown (1985). Although Koretsky et al. (1998) did not provide illustrations of the inferred edge surface topologies, it appears from the site types they predicted that they likely chose to terminate these edge faces along the same planes predicted by crystal growth theory. As with Bleam et al. (1993), they did not allow for surface relaxation.

We have chosen to interpret our results within the framework of the type of model articulated by White and Zelazny (1988). As shown below, allowing for charge neutralization via surface relaxation at some edge surface sites provides us with a rationale for the exceptionally low reactivity of the preferred growth faces on nontronite. Specifically, the O atoms connecting between the octahedral and tetrahedral sheets (hereafter designated "connecting O atoms") on dioctahedral phyllosilicates are predicted to be fully bonded, and hence less reactive with respect to proton attack. However, some of the connecting O atoms at kink sites on broken edges and the connecting O atoms on trioctahedral edge faces are predicted to be underbonded. To show that this is the case, Hartman-Perdock crystal growth theory is applied below to predict the topology of all the relevant edge surfaces.

Hartman-Perdock crystal growth theory. Hartman and Perdock (1955a, 1955b, 1955c) proposed that the typical morphology of crystals could be explained in terms of bond energies. Crystal growth is approximated as the formation of strong bonds between growth units of stoichiometric composition (Grim and Güven 1978), and growth faces are observed to lie parallel to one or more continuous chains of strong bonds within the crystal structure, called Periodic Bond Chains (PBCs). It must be possible to divide the entire crystal structure into PBCs of stoichiometric composition, which have no bonds in common, and a PBC must not entirely consist of periods of other PBCs. Planes parallel to two or more PBCs exhibit a low surface energy configuration, which results in a prominent, flat (F) face. Faces parallel to one PBC are stepped (S), and are less prominent than F faces. Kinked (K) faces are parallel to no PBCs, and due to their high surface energy, usually do not occur as growth surfaces.

The topology of the predicted F and S surfaces may be inferred by assuming that they are terminated along the sides of the stoichiometric PBCs. However, Grim and Güven (1978) pointed out that one cannot realistically impose the condition of stoichiometry on such a complex structure, and instead defined separate PBCs along chains of oxygen-linked tetrahedral and octahedral cations. For the purpose of defining edge surface topology, in this paper we will adhere to the condition of stoichiometry with respect to the phyllosilicate T-O-T layers, unless a particularly high-energy surface is generated. In addition, all edge surface sites will be terminated with O atoms or OH groups.

Prediction of edge surface topology. White and Zelazny (1988) began their analysis of dioctahedral edge surface structure by defining the minimum stoichiometric units required for crystal growth, according to PBC theory. (Obviously this is somewhat of an oversimplification of the actual crystal growth process.) For 2:1 dioctahedral phyllosilicates without ordered substitution, this may be represented by two tetrahedra connected to a single octahedron, neglecting interlayer cations. The tetrahedron connected to the top of the octahedron is related to the tetrahedron connected to the bottom by a center of symmetry, so as not to create a dipole (see Fig. 4). Grim and Güven (1978) and Hartman (1982) showed that the PBCs in phyllosilicates are along the [1$\bar{1}$0], [100] and [110] directions, so that a flat (001) face is predicted, as well as stepped (110), (010), and (1$\bar{1}$0) edge growth faces. Consistent with this, atomically flat (001) faces dominate phyllosilicate crystal habits, and the predicted edge faces are the "pseudohexagonal" faces normally observed on euhedral phyllosilicate crystals. The fundamental crystal growth units are linked together in the PBCs schematically represented by polyhedral models (Fig. 5), and by ball and stick models of the PBCs, viewed parallel to the chain directions (Fig. 6). From Figure 6, edge faces terminated on either side of the chains would result in an equivalent topology. Also, the chains parallel to the (110) and (1$\bar{1}$0) edge faces are symmetrically equivalent, so only the chain parallel to (110) is depicted here.

Bleam et al. (1993) suggested that the previous workers neglected to describe two important PBCs in the phyllosilicate structure, parallel to the (100) and (130) edge faces. They supported this assertion by citing Sun and Baronnet (1989a, 1989b), who reported synthetically grown phlogopite crystals with (100) and (130) faces. However, a closer analysis of phyllosilicate structures shows that the bond chains parallel to (100) and (130) are what Hartman and Perdock (1955b) called "zigzag chains," composed entirely of periods of other PBCs. On the other hand, perhaps in this case it is more realistic to do as Grim and Güven (1978) suggest, and separate the 2:1 layers into individual tetrahedral and octahedral sheets for PBC analysis. In this case the PBCs parallel to (100) and (130) in the dioctahedral structure would clearly be zigzag chains, whereas the equivalent PBCs in the trioctahedral structure would be zigzagged in the tetrahedral sheets, but straight in the octahedral sheet. Therefore, one might assume that faces terminated along the bond chains parallel to (100) and (130) in trioctahedral structures would be more stable than K faces, but less stable than true S faces such as (010), (110), and (1$\bar{1}$0). This conclusion also seems consistent with Sun and Baronnet's results, where the (100) and (130) forms were important only close to equilibrium (Sun and Baronnet 1989a) and where Cr inhibited crystal growth at these faces (Sun and Baronnet 1989b). However, as noted above, in this study surfaces parallel to (100) were observed to occur on a few laths of nontronite, which is a dioctahedral mineral. Rather than growth surfaces, these were probably broken edge surfaces perpendicular to the length of the laths, and to our knowledge (100) growth faces have never been unambiguously identified on dioctahedral phyllosilicate minerals. This fact appears to support the judgement of previous workers in choosing not to identify PBCs parallel to these surfaces in dioctahedral structures (White and Zelazny 1988; Grim and Güven 1978; and Hartman 1982).

The "zigzag" nature of the chains parallel to (100) and (130) in a dioctahedral structure can be clearly seen by examining the polyhedral representations. In Figure 7, a dioctahedral sheet structure is viewed perpendicular to the (001) plane, and tetrahedral elements of the bond chains parallel to (010), (110),

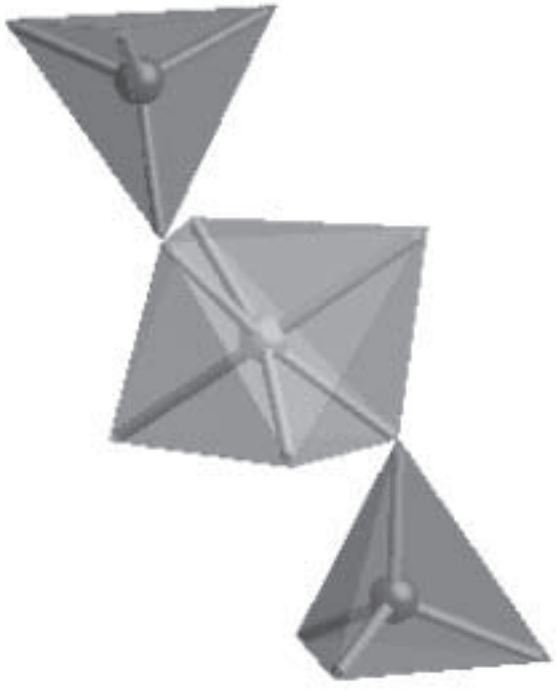

FIGURE 4. One stoichiometric crystal growth unit for a dioctahedral 2:1 phyllosilicate, assuming random substitutions.

($1\bar{1}0$), and (100) are highlighted. The chain of bonds parallel to (100) is composed exclusively of elements of the PBCs parallel to (010), (110), and ($1\bar{1}0$). An identical result is obtained by examining the octahedral elements of these bond chains, and Figure 8 shows the same to be true for the chain parallel to (130).

Application of PBC theory to trioctahedral phyllosilicates is somewhat more complex. To maintain stoichiometry, the minimum growth unit for a trioctahedral T-O-T layer must consist of four tetrahedra and three octahedra, including two M2 and one M1 sites (see Fig. 9). Ball and stick models of the PBCs, viewed parallel to the chain directions (Fig. 10a) show that terminating edge faces on either side of the (110) and ($1\bar{1}0$) chains would result in an equivalent topology of edge surface sites. Figure 10b shows that terminating edge surfaces on either side of the (010) chain would result in two very different edge site topologies. Whereas one side would be equivalent to the (010) face of a dioctahedral phyllosilicate, the other would have M1 octahedra protruding from the surface. However, a tally of the type and number of bonds severed to generate such surfaces reveals that two more Si-O bonds per unit cell repeat would have to be broken to generate a surface with protruding M1 octahedra than to generate one without. Therefore, our analysis assumes that stable (010) surfaces on trioctahedral phyllosilicates have an edge surface site topology equivalent to that of a (010) face on a dioctahedral phyllosilicate.

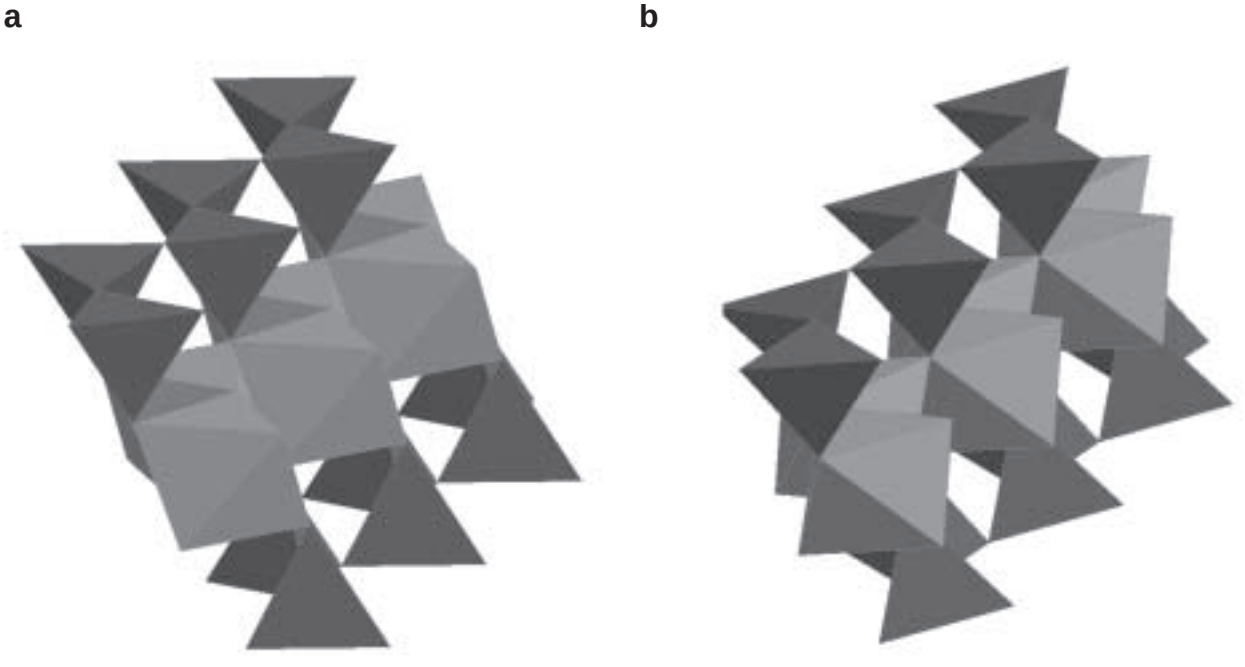

FIGURE 5. Stoichiometric Periodic Bond Chains (PBCs) for a dioctahedral 2:1 phyllosilicate. (**a**) Chain running parallel to the (110) face. The ($1\bar{1}0$) face is symmetrically equivalent. (**b**) Chain running parallel to the (010) face.

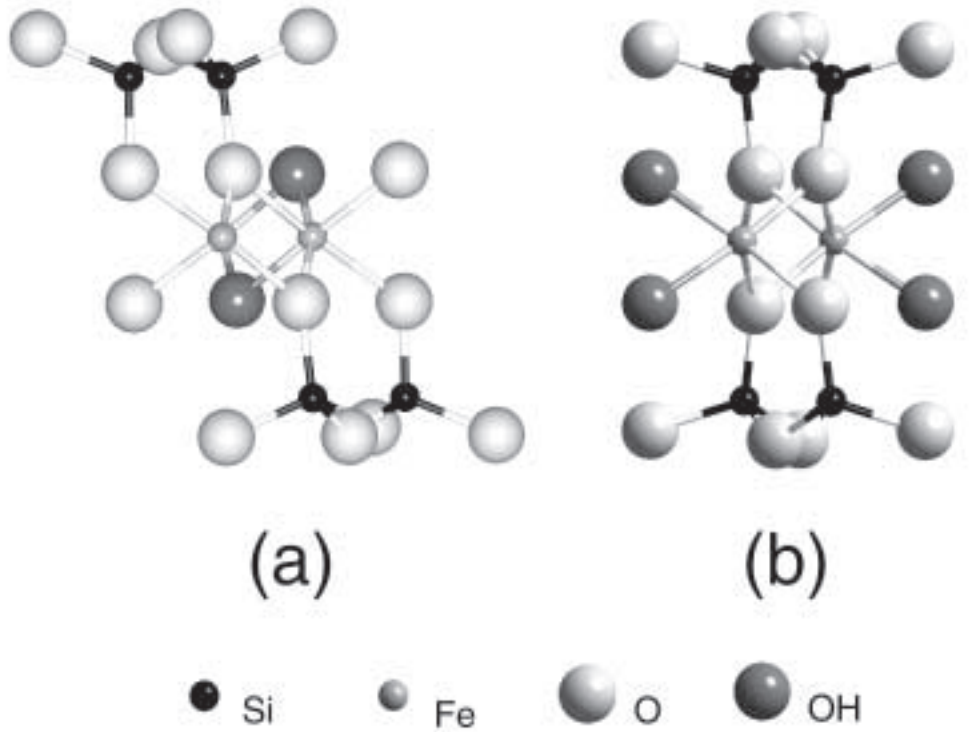

FIGURE 6. Ball and stick models of the Periodic Bond Chains (PBCs) in Figure 5, viewed parallel to the PBC vector. (**a**) Chain parallel to the (110) face. The (1$\bar{1}$0) face would be symmetrically equivalent. (**b**) Chain parallel to the (010) face.

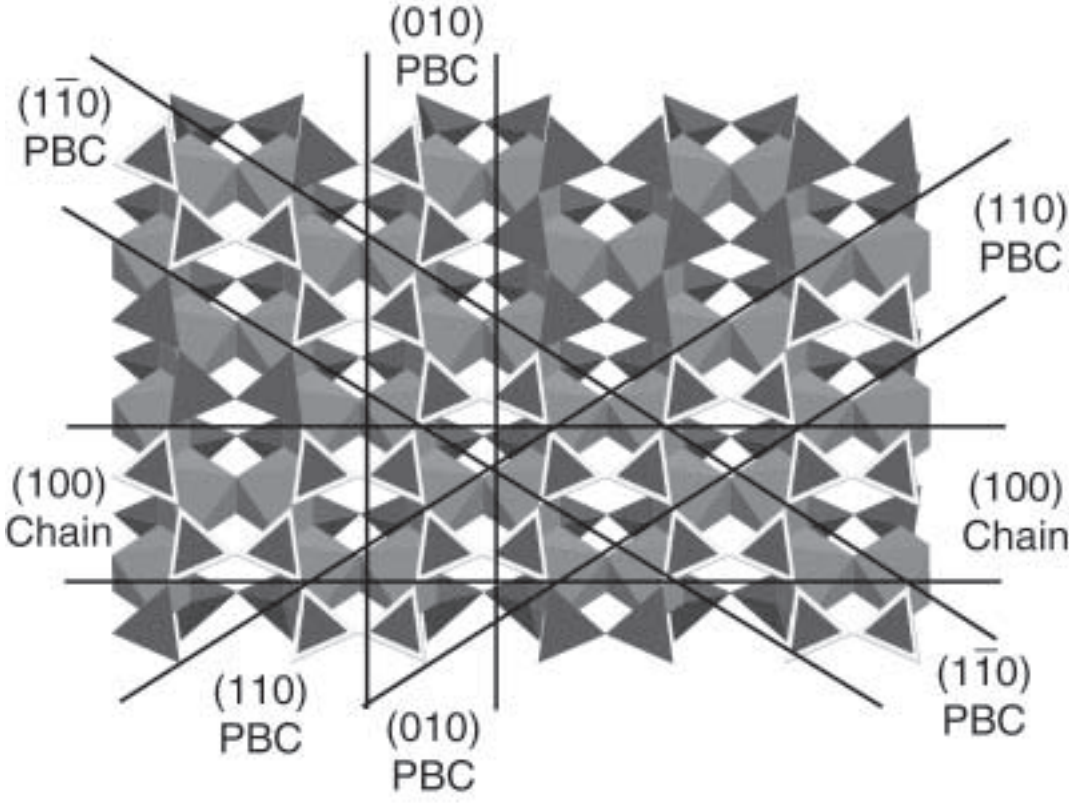

FIGURE 7. Polyhedral representation of a dioctahedral T-O-T layer. The highlighted tetrahedra are part of the bond chains indicated in the figure. It can clearly be seen that the chain parallel to the (100) face is composed entirely of elements of the (110), (1$\bar{1}$0), and (010) Periodic Bond Chains (PBCs). Thus, (100) should not be treated as a PBC.

Surface relaxation and observed reactivity. The assumption that surface sites with unsaturated valency are more reactive than fully saturated sites, using various methods for calculating bond valence, has commonly been used to explain the differential reactivity of crystal faces (e.g., van Santen 1982; Ziolkowski 1986; Bleam 1993; Bargar et al. 1997; Towle et al. 1999a, 1999b), with at least qualitative success. We will make the same assumption here to rationalize the observed reactivity of the nontronite and hectorite edge faces. Simple Pauling bond strengths will be used, where $\zeta = \sum_i \frac{Z_i}{v_i}$. In this equation, z is the total bond strength coordinating each O or OH surface site, Z_i is the valence of each cation coordinating the site, and v_i is the coordination number of each cation.

Table 1 summarizes all the sites available on the surfaces of edge faces of nontronite and hectorite, terminated by the PBCs discussed above. Because we make generalizations about the reactivity of distinct crystal faces, we ignore the effects of isomorphous substitutions (see White and Zelazny 1988). Thus, ideal structures with only one type of tetrahedral cation (Si^{4+}) and one type of octahedral cation (Fe^{3+} or Mg^{2+}) are included.

In the nontronite structure, the 2-coordinated connecting O atoms on the (110) and (1$\bar{1}$0) edge faces are situated adjacent to 1-coordinated O atoms bonded to octahedral Fe. White and Zelazny (1988) suggested that if the 1-coordinated O were doubly protonated, this Fe-O bond might lengthen out to a bond strength of near 0, resulting in an uncharged bound water site. Simultaneously, the bonds to the adjacent 2-coordinated connecting O would shorten, raising the total bond strength reaching this site to 2, leaving the 2-coordinated oxygen fully charge-satisfied. Given that at pH values between approximately 3 and 9 the silanol groups on these edge faces would be singly protonated, leaving these sites fully charge-satisfied, these faces would normally be uncharged. However, even at extreme pH levels, the connecting O sites would remain uncharged, and thus would have a very low affinity for adsorbing protons. On the nontronite (010) faces, all surface sites are fully bonded, except for adjacent 1-coordinated OHs bonded to octahedral cations. Each of these is underbonded by 1/2, and when doubly protonated, they would be overbonded by 1/2. Again, however, the connecting O sites are fully bonded, and would have a very low affinity for adsorbing protons.

White and Zelazny (1988) justified their speculations about the surface relaxation discussed above by citing similar phenomena known to occur at the edge surfaces of sepiolite and palygorskite (Preisinger 1959), and by the ability of their model to successfully predict observed anomalies in structural formulae calculated for fine-grained clay minerals. In addition, Childs et al. (1999) recently observed the presence of five-coordinated Al in allophane using nuclear magnetic resonance spectroscopy, and suggested these might originate at the edges of incomplete octahedral layers. Because the proposed bond shifts on dioctahedral clay edge surfaces would effectively result in 5-coordinated octahedral cations, such observations may be significant to White and Zelazny's case. In the case of nontronite,

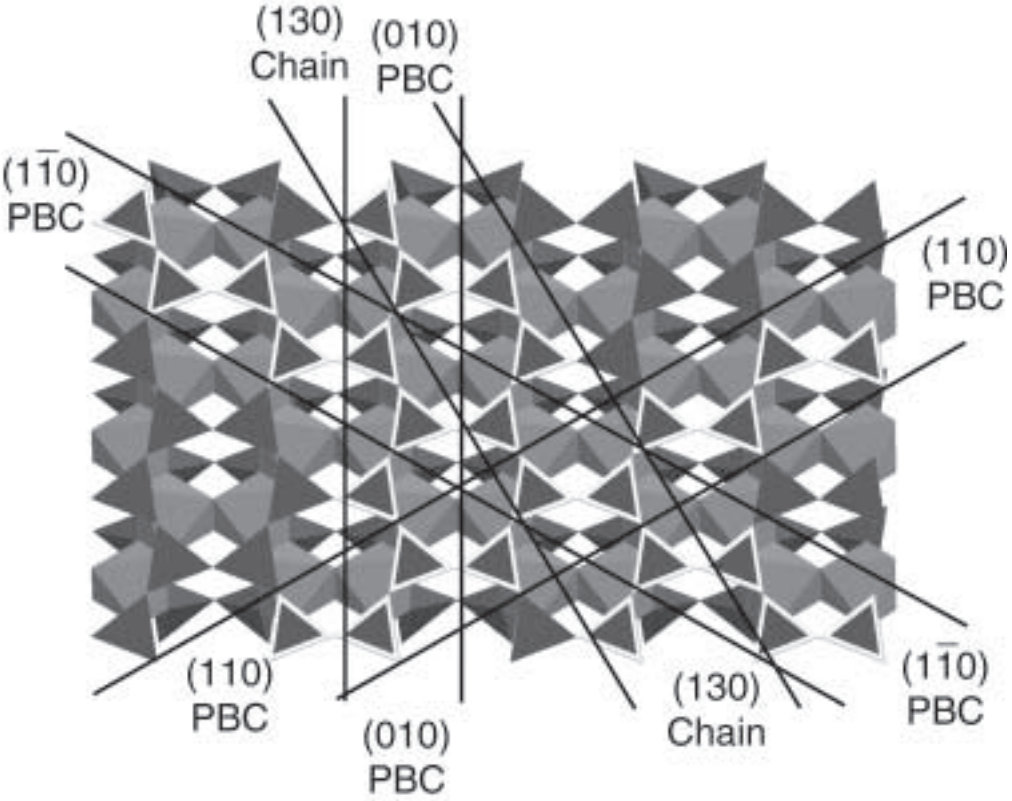

FIGURE 8. Polyhedral representation of a dioctahedral T-O-T layer. The highlighted tetrahedra are part of the bond chains as indicated. The chain parallel to the (130) face is composed entirely of elements of the (110), (1$\bar{1}$0), and (010) Periodic Bond Chains (PBCs). Thus, (130) should not be treated as a PBC.

even in the bulk the octahedral sheet is severely distorted, with Fe-O bond lengths ranging from 1.815 to 2.062 Å, corresponding to empirically determined bond strengths of 0.86 to 0.44 (Altermatt and Brown 1985). This suggests that the proposed bond shifts would not be out of the question. Beyond these simple arguments, molecular modeling calculations are needed to theoretically justify the predicted surface relaxation.

In contrast, cutting our crystal models along noneuhedral planes to simulate broken edges yielded numerous kink sites, often including underbonded connecting O atoms coordinated to an octahedral cation surrounded by at least two other underbonded anion sites. In such cases we would not expect a complete neutralization of the surface charge.

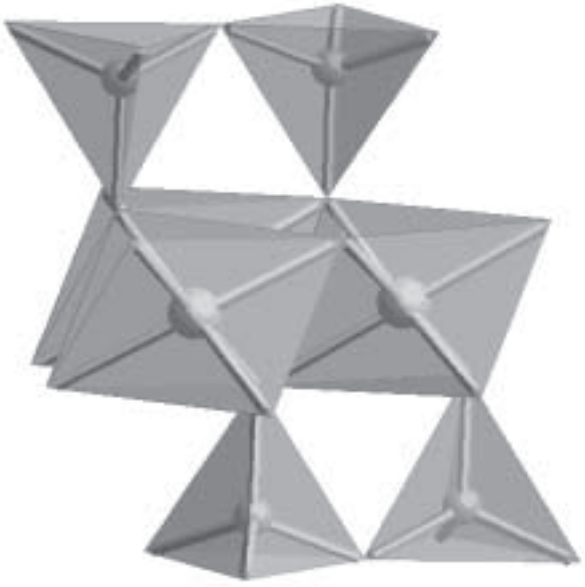

FIGURE 9. One stoichiometric crystal growth unit for a trioctahedral 2:1 phyllosilicate, assuming random substitutions.

Similarly, on both the (010), (110), and (1$\bar{1}$0) edge faces of hectorite, the underbonded connecting O atoms are bonded to octahedral cations which are also bonded to another undersaturated O. The total strength of bonds (Pauling) coordinating each of these O atoms is 5/3, so shifting a 1/3 charge from one site to the other would still leave one of the sites underbonded. Therefore, we would not expect complete autocompensation of the surface charge on these faces, either.

If it is assumed that the slowest step in the dissolution process of nontronite and hectorite is the breaking of connecting oxygen bonds between the octahedral and tetrahedral sheets, the observed differential reactivity is readily explained. That is, all the faces which dissolve relatively quickly, including all the hectorite edge surfaces and nontronite broken edges, are predicted to have coordinatively unsaturated connecting O atoms, which would have a high affinity for attacking protons. The faces observed to dissolve much more slowly, including nontronite (010), (110), and (1$\bar{1}$0), are predicted to have fully charge-satisfied connecting O atoms with a much lower affinity for protonation. At first glance, the stability of the edge surfaces (broken edges?) parallel to (100) on the nontronite laths appears to be something of an anomaly, because PBC theory predicts that they should be K faces. However, the "zigzag chains" that run parallel to this face are composed of elements of the PBCs parallel to the (010), (110), and (1$\bar{1}$0) edge surfaces, which have fully bonded connecting O atoms. Thus, it

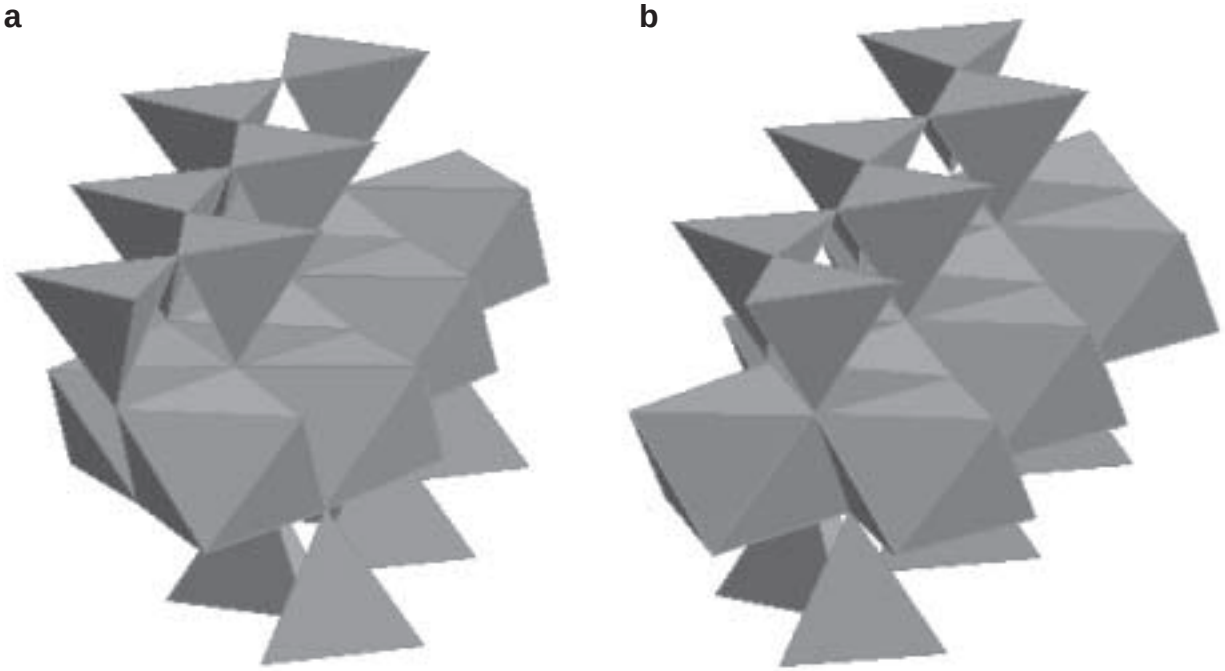

FIGURE 10. Ball and stick models of the Periodic Bond Chains (PBCs) in Figure 10, viewed parallel to the PBC vector. (**a**) Chain parallel to the (110) face. The (1$\bar{1}$0) face would be symmetrically equivalent. (**b**) Chain parallel to the (010) face.

TABLE 1. Site types and densities on nontronite and hectorite edge faces

Site type	Coordinating atoms	Coordinating bond strength	Sites per unit cell face	Sites per nm^2
		Nontronite (110) and (1$\bar{1}$0)		
O	Si	1	4	3.76
O	2 Si	2	8	7.53
O	Si, 2 Fe	2	2	1.88
O	Si, Fe	3/2*	2	1.88
O	Fe	1/2†	2	1.88
OH	2 Fe	1	2	1.88
		Nontronite (010)		
O	Si	1	2	3.80
O	2 Si	2	4	7.59
O	Si, 2 Fe	2	2	3.80
OH	Fe	1/2	2	3.80
		Hectorite (110) and (1$\bar{1}$0)		
O	Si	1	4	3.70
O	2 Si	2	8	7.41
O	Si, 2 Mg	5/3	2	1.85
O	Mg	1/3	2	1.85
OH	2 Mg	2/3	2	1.85
OH	Mg	1/3	2	1.85
		Hectorite (010)		
O	Si	1	2	3.94
O	2 Si	2	4	7.89
O	Si, 2 Mg	5/3	2	3.94
OH	Mg	1/3	2	3.94

* These bonds are predicted to shorten, so that the coordinating bond strenth will total 2.
† These bonds are predicted to lengthen to bond strength 0, so that when the site is doubly protonated, it will be a bound water.

seems to follow that (100) edge surfaces might exhibit low reactivity, but established dissolution fronts likely would not show a tendency to become pinned at a K face.

Implications for the mechanism of proton attack

The conclusion that the dissolution rate is controlled by the breaking of bonds to connecting O atoms between the tetrahedral and octahedral sheets seems inconsistent with the model of kaolinite dissolution proposed by Wieland and Stumm (1992). In their study, Wieland and Stumm measured the surface protonation of kaolinite via potentiometric titration, as well as the dissolution rate, in acidic and basic solutions. They interpreted their results within the framework of the coordinative chemical model of mineral dissolution developed by Furrer and Stumm (1986) and Wieland et al. (1988), where dissolution rates of simple oxides in acidic solutions were shown to be proportional to integral orders of the concentration of protonated surface species. It was assumed that these integral orders corresponded to the stoichiometry of a precursor to the rate-controlling activated complex for the dissolution reaction. In the case of kaolinite, Wieland and Stumm (1992) found that the dissolution rate of the edge surfaces in acid solution could be modeled as a first-order function of the concentration of protonated aluminol sites on the edge faces of the mineral. They concluded that the activated complex controlling the dissolution reaction at the kaolinite edge surface had a stoichiometry of 1 H to 1 Al. Such a model seems to implicitly assume that all protonated surface groups associated with the octahedral cations are equally reactive. However, Wieland and Stumm (1992) realized that "precursor configurations" associated with different surface functional groups might have very different surface energies, but appealed to Monte-Carlo simulations which showed that the surface of a dissolving mineral will tend toward a configuration with only one type of surface complex (Wehrli 1989). Wieland and Stumm's (1992) explanation remains inconsistent with ours, because if the rate-determining step is associated with the hydrolysis of connecting O bonds, rather than easily protonated, monodentate aluminol groups, there should be no such direct link between total surface protonation on aluminol groups and the rate-determining activated complex.

In the case of nontronite dissolution, one cannot explain the tendency for the reaction front to become pinned at the pseudohexagonal face angles in terms of a minimization of protonated surface functional groups associated with the octahedral cations. Such an explanation might suffice for the (110) and (1$\bar{1}$0) edge faces, which likely have no such readily protonated surface functional groups, but not for the (010) faces, which have a reasonably high density of amphoteric, monodentate groups coordinated to an octahedral cation. Whereas the density of these sites on the (010) edge faces is almost certainly lower than on most broken edges, the difference cannot be so great as to explain the much, much slower dissolution of the nontronite (010) faces.

Another problem with the model proposed by Wieland and Stumm (1992) is that ab initio calculations performed by Xiao and Lasaga (1994) predicted the key step in the dissolution of Si-O-Al groups would be proton adsorption on the connecting O atoms. Also, an adsorbed proton on one Si-O-Al group was not predicted to significantly affect the dissolution reaction on neighboring groups. Therefore, the protonation of amphoteric, monodentate surface functional groups on such surfaces should

not control their dissolution rates.

Our explanation of the in situ observations of nontronite and hectorite dissolution is consistent with the model of proton attack at the edge surfaces of kaolinite proposed by Ganor et al. (1995). They found that, within experimental error, kaolinite dissolution rates in acid solutions were first order with respect to the *total* surface protonation. A model of kaolinite dissolution was proposed, where the rate-controlling step is the sequential breaking of bonds to connecting O atoms. They explained the linear dependence of the rates on total surface proton concentration by assuming equilibrium between the various types of surface protonated sites. Assuming the activity coefficients and concentrations of the surface species are reasonably constant during the dissolution reaction, this results in a first-order reaction with respect to total surface proton concentration. In a similar study, Zysset and Schindler (1996) showed that the proton-promoted dissolution of montmorillonite is first order with respect to total surface proton concentration, including protons inferred to have exchanged into the interlayer spaces of the mineral. They proposed that the dissolution rate is controlled by hydrolysis of either Si-O-Al or Al-OH-Al bonds, and that protons adsorbed anywhere on the montmorillonite surface can quickly diffuse to the active sites. This explanation appears to be nearly equivalent, at least qualitatively, to the one proposed by Ganor et al. (1995). However, the possibility that the breaking of bonds between octahedral sites controls the dissolution rate can be excluded on the basis of the hectorite dissolution data reported by Bosbach et al. (2000), who showed that the step retreat rate for hectorite was much slower than that for brucite (Jordan and Rammensee 1996).

ACKNOWLEDGMENTS

We thank Michel Schlegel for preparing the hectorite suspension, and Alain Baronnet and G. Norman White for helpful reviews of the manuscript. B.B., M.H., and E.R. are grateful for the support of the National Science Foundation (EAR-9628023, EAR-9902996, and the Graduate Student Fellowship program) and the Petroleum Research Fund administered by the American Chemical Society (ACS-PRF 31598-AC2 and ACS-PRF 34326-AC2). D.B. and L.C. are grateful for financial support by the Deutscher Akademischer Austauschdienst and the French Ministery of Foreign affairs.

REFERENCES CITED

Altermatt, D. and Brown, I.D. (1985) Bond-valence parameters obtained from a systematic analysis of the inorganic crystal structure database. Acta Crystallographica, B41, 244–247.

Anderson, S.J. and Sposito, G. (1991) Cesium-adsorption method for measuring accessible structural surface charge. Soil Science Society of America Journal, 55, 1569–1576.

Bargar, J.R., Towle, S.N., Brown, G.E., Jr., and Parks, G.A. (1997) XAFS and bond-valence determination of the structures and compositions of surface functional groups and Pb(II) and Co(II) sorption products on single-crystal a-Al_2O_3. Journal of Colloid and Interface Science, 185, 473–492.

Barrett, S.D. (1997) Image analysis and the internet. Scientific Data Management, 1, 18–25.

Besson, G., de la Calle, C., Rautureau, M., Tchoubar, C., Tsipurski, S.I., and Drits, V.A. (1982) X-ray and electron diffraction study of the structure of the Garfield nontronite. Developments in Sedimentology, 35, 29–40.

Besson, G., Bookin, A.S., Dainyak, L.G., Rautureau, M., Tsipursky, S.I., Tchoubar, C., and Drits, V.A. (1983) Use of diffraction and Mössbauer methods for the structural and crystallochemical characterization of nontronites. Journal of Applied Crystallography, 16, 374–383.

Bickmore, B.R., Hochella, M.F., Jr., Bosbach, D., and Charlet, L. (1999a) Methods for performing Atomic Force Microscopy imaging of clay minerals in aqueous solutions. Clays and Clay Minerals, 47, 573–581.

Bickmore, B.R., Rufe, E., Barrett, S.D., and Hochella, M.F., Jr. (1999b) Measuring discrete feature dimensions in AFM images with Image SXM. Geological Materials Research, 1, n.5. See http://gmr.minsocam.org

Bleam, W.F. (1993) Atomic theories of phyllosilicates: Quantum chemistry, statistical mechanics, electrostatic theory, and crystal chemistry. Reviews of Geophysics, 31, 51–73.

Bleam, W.F., Welhouse, G.J., and Janowiak, M.A. (1993) The surface Coulomb energy and proton Coulomb potentials of pyrophyllite {010}, {110}, {100}, and {130} edges. Clays and Clay Minerals, 41, 305–316.

Bloss, F.D., Shekarchi, E., and Shell, H.R. (1959) Hardness of synthetic and natural micas. American Mineralogist, 44, 33–48.

Boisen, M.B. and Gibbs, G.V. (1985) Mathematical Crystallography, Reviews in Mineralogy 15, 460 p. The Mineralogical Society of America, Washington, D.C.

Bonnin, D., Calas, G., Suquet, H., and Pezerat, H. (1985) Sites occupancy of Fe^{3+} in Garfield nontronite: A spectroscopic study. Physics and Chemistry of Minerals, 12, 55–64.

Bosbach, D. and Hochella, M.F. Jr. (1996) Gypsum growth in the presence of growth inhibitors: a scanning force microscopy study. Chemical Geology, 132, 227–236.

Bosbach, D. and Rammensee, W. (1994) In situ investigation of growth and dissolution on the (010) surface of gypsum by Scanning Force Microscopy. Geochimica et Cosmochimica Acta, 58, 843–849.

Bosbach, D., Jordan, G., and Rammensee, W. (1995) Crystal growth and dissolution kinetics of gypsum and fluorite: An in situ Scanning Force Microscope study. European Journal of Mineralogy, 7, 267–278.

Bosbach, D., Junta-Rosso, J.L., Becker, U., and Hochella, M.F. Jr. (1996) Gypsum growth in the presence of background electrolytes studied by Scanning Force Microscopy. Geochimica et Cosmochimica Acta, 60, 3295–3304.

Bosbach, D., Hall, C., and Putnis, A. (1998) Mineral precipitation and dissolution in aqueous solution: in-situ microscopic observations on barite (001) with atomic force microscopy. Chemical Geology, 151, 143–160.

Bosbach, D., Charlet, L., Bickmore, B.R., and Hochella, M.F. Jr. (2000) The dissolution of hectorite: In-situ, real-time observations using Atomic Force Microscopy. American Mineralogist, 85, 1209–1216.

Brady, P.V., Cygan, R.T., and Nagy, K.L. (1996) Molecular controls on kaolinite surface charge. Journal of Colloid and Interface Science, 183, 356–364.

Brauer, K.-H. (1971) Ätzresultate an Kristallen der Glimmergruppe, p. 1–116. Akademie-Verlag, Berlin.

Charlet, L., Schindler, P.W., Spadini, L., Furrer, G., and Zysset, M. (1993) Cation adsorption on oxides and clays—the Aluminum case. Aquatic Sciences, 55, 291–303.

Childs, C.W., Hayashi, S., and Newman, R.H. (1999) Five-coordinate aluminum in allophane. Clays and Clay Minerals, 47, 64–69.

Deer, W.A., Howie, R.A., and Zussman, J. (1992) An Introduction to the Rock-Forming Minerals, 2nd edition, Longman Scientific & Technical, Essex, U.K.

Dove, P. and Chermak, J. (1994) Mineral-water interactions: Fluid cell applications of scanning force microscopy. In K.L. Nagy and A.E. Blum, Eds. Scanning Probe Microscopy of Clay Minerals, p. 139–169. The Clay Minerals Society, Boulder, Colorado.

Dove, P.M. and Hochella, M.F. Jr. (1993) Calcite precipitation mechanisms and inhibition by orthophosphate: In situ observations by Scanning Force Microscopy. Geochimica et Cosmochimica Acta, 57, 705–714.

Drake, B., Prater, C.B., Weisenhorn, A.L., Gould, S.A.C., Albrecht, T.R., Quate, C.F., Cannell, D.S., Hansma, H.G., and Hansma, P.K. (1989) Imaging crystals, polymers, and processes in water with the atomic force microscope. Science, 243, 1586–1588.

Eggleton, R.A. (1977) Nontronite: Chemistry and X-ray diffraction. Clay Minerals, 12, 181.

Eslinger, E. and Pevear, D. (1988) Clay Minerals for Petroleum Geologists and Engineers. Society of Economic Paleontologists and Mineralogists.

Fouke, B.W. and Reeder, R.J. (1992) Surface structural controls on dolomite composition: Evidence from sectoral zoning. Geochimica et Cosmochimica Acta, 56, 4015–4024.

Furrer, G. and Stumm, W. (1986) The coordination chemistry of weathering: I. Dissolution kinetics of *d*-Al_2O_3 and BeO. Geochimica et Cosmochimica Acta, 50, 1847–1860.

Ganor, J., Mogollón, J.L., and Lasaga, A.C. (1995) The effect of pH on kaolinite dissolution rates and on activation energy. Geochimica et Cosmochimica Acta, 59, 1037–1052.

Grantham, M.C. and Dove, P.M. (1996) Investigation of bacterial-mineral interactions using Fluid Tapping Mode Atomic Force Microscopy. Geochimica et Cosmochimica Acta, 60, 2473–2480.

Grim, R.E. and Güven, N. (1978) Bentonites. Geology, Mineralogy, Properties and uses. Developments in Sedimentology, 24. Elsevier, Amsterdam.

Güven, N. (1988) Smectites. In S.W. Bailey, Ed. Hydrous phyllosilicates. Reviews in Mineralogy 19. Mineralogical Society of America. Washington D.C.

——(1991) Smectites. In S.W. Bailey, Ed., Hydrous Phyllosilicates, 19, p. 497–560. Reviews in Mineralogy, Mineralogical Society of America, Washington, D.C.

Hansma, P.K., Cleveland, J.P., Radmacher, M., Walters, D.A., Hillner, P.E., Bezanilla, M., Fritz, M., Vie, D., Hansma, H.G., Prater, C.B., Massie, J., Fukunaga, L., Gurley, J., and Elings, V. (1994) Tapping mode atomic force microscopy in liquids. Applied Physics Letters, 64, 1738–1740.

Hartman, P. (1963) Structure, growth and morphology of crystals. Zeitschrift für

Krystallographie, 119, 65–78.
——(1973) Structure and morphology. In P. Hartman, Ed., Crystal Growth: An Introduction, p. 367–402. North Holland Publishing Company, Amsterdam.
——(1978) On the validity of the Donnay-Harker Law. Canadian Mineralogist, 16, 387–391.
——(1982) On the growth of dolomite and kaolinite crystals. Neues Jahrbuch für Mineralogie, Monatshefte 1982, 84–92.
Hartman, P. and Perdock, W.G. (1955a) On the relations between structure and morphology of crystals. I. Acta Crystallographica, 8, 49–52.
——(1955b) On the relations between structure and morphology of crystals. II. Acta Crystallographica, 8, 521–524.
Hartman, P. and Perdock, W.G. (1955c) On the relations between structure and morphology of crystals. III. Acta Crystallographica, 8, 525–529.
Hillner, P.E., Gratz, A.J., Manne, S., and Hansma, P.K. (1992) Atomic-Scale imaging of calcite and dissolution in real time. Geology, 20, 359–362.
Hochella, M.F. Jr. (1990) Atomic structure, microtopography, composition, and reactivity of mineral surfaces. In M.F. Hochella, Jr. and A.F. White, Eds., Mineral-Water Interface Geochemistry, 23, p. 87–132. Reviews in Mineralogy, The Mineralogical Society of America, Washington, D.C.
——(1995) Mineral surfaces: Their characterization and their chemical, physical and reactive nature. In D.J. Vaughan and R.A.D. Pattrick, Eds., Mineral Surfaces, p. 17–60. Chapman and Hall, London.
Hochella, M.F. Jr., Rakovan, J., Rosso, K., Bickmore, B., and Rufe, E. (1998) New directions in mineral surface geochemical research using scanning probe microscopy. In D.L. Sparks and T.J. Grundl, Eds., Mineral-Water Interfacial Reactions: Kinetics and Mechanisms, ACS Symposium Series Vol. 715, p. 37–56. American Chemical Society, Washington, D.C.
Johnson, C.A. (1995) Applications of scanning probe microscopy part 4: AFM imaging in fluids for the study of colloidal particle adsorption. American Laboratory, 27, 12.
Jordan, G. and Rammensee, W. (1996) Dissolution rates and activation energy for dissolution of brucite (001): A new method based on the microtopography of crystal surfaces. Geochimica et Cosmochimica Acta, 60, 5055–5062.
Junta, J.L. and Hochella, M.F. Jr. (1994) Manganese (II) oxidation at mineral surfaces: A microscopic and spectroscopic study. Geochimica et Cosmochimica Acta, 58, 4985–4999.
Junta-Rosso, J.L, Hochella, M.F. Jr., and Rimstidt, J.D. (1997) Linking microscopic and macroscopic data for heterogeneous reactions illustrated by the oxidation of manganese (II) at mineral surfaces. Geochimica et Cosmochimica Acta, 61, 149–159.
Kadi-Hanifi, M. and Méring, J. (1972) Précisions sur la structure de l'hectorite. C.R. Acad. Sc. Paris, Série D, 274, 149–151.
Kaviratna, H. and Pinnavaia, T.J. (1994) Acid hydrolysis of octahedral Mg^{2+} sites in 2:1 layered silicates: An assessment of edge attack and gallery access mechanisms. Clays and Clay Minerals, 42, 717–723.
Klein, C. and Hurlbut, C.S. Jr. (1993) Manual of Mineralogy, 21st ed., 681 p. Wiley, New York.
Koretsky, C.M., Sverjensky, D.A., and Sahai, N. (1998) A model of surface site types on oxide and silicate minerals based on crystal chemistry: Implications for site types and densities, multi-site adsorption, surface infrared spectroscopy, and dissolution kinetics. American Journal of Science, 298, 349–438.
Liang, Y., Baer, D.R., McCoy, J.M., Amonette, J.E., and LaFemina, J.P. (1996) Dissolution kinetics at the calcite-water interface. Geochimica et Cosmochimica Acta, 60, 4883–4887.
Manceau, A., Chateigner, D., and Gates, W.P. (1998) Polarized EXAFS, distance-valence least-squares modeling (DVLS), and quantitative texture analysis approaches to the structural refinement of Garfield nontronite. Physics and Chemistry of Minerals, 25, 347–365.
Muljadi, D., Posner, A.M., and Quirk, J.P. (1966) The mechanism of phosphate adsorption by kaolinite, gibbsite, and pseudoboehmite. Journal of Soil Science, 17, 212–247.
Murad, E. (1987) Mössbauer spectra of nontronites: structural implications and characterization of associated iron oxides. Zeits. Pflanzenernaehr. Bodenk. 150, 279–285.
Nagy, K.L. (1995) Dissolution and precipitation kinetics of sheet silicates. In A.F. White and S.L. Brantley, Eds., Chemical Weathering Rates of Silicate Minerals, 31, p. 173–233. Reviews in Mineralogy, Mineralogical Society of America, Washington, D.C.
Nagy, K.L. and Blum, A.E., Eds. (1994) Scanning Probe Microscopy of Clay Minerals, CMS Workshop Lectures vol. 7, 239 p. Clay Minerals Society, Boulder, Colorado.
Oberlin, P.A. and Méring, J. (1966) Observations sur l'hectorite (etude en microscopie et diffraction electroniques). Bulletin de la Société Française de Mineralogie et cristallographie, LXXXIX, 29–40.
Palmer, D.(1998) CrystalMaker: Interactive Crystallography for Macintosh. Holywell Press, Cambridge, U.K.
Pandya, N.S. and Pandya, J.R. (1959) Etching of mica by fused alkalies. Bulletin of the National Institute of Sciences of India, 14, 148–151.
Paquette, J. and Reeder, R.J. (1990) New type of compositional zoning in calcite: Insights into crystal-growth mechanisms. Geology, 18, 1244–1247.
Park, N.-S., Kim, M.-W., Langford, S.C., and Dickinson, J.T. (1996) Atomic layer wear of single-crystal calcite in aqueous solution using scanning force microscopy. Journal of Applied Physics, 80, 2680–2686.
Patel, A.R. and Ramanathan, S. (1962) Etching Mica Cleavages. Acta Crystallographica, 15, 860–862.
Preisinger, A. (1959) X-ray study of the structure of sepiolite. In A. Swineford, Ed., Clays and Clay Minerals, Proceedings of the 6th National Conference, Berkeley, California, 1957, p. 61–67. Pergamon Press, New York.
Putnis, A., Junta-Rosso, J.L., and Hochella, M.F. Jr. (1995) Dissolution of barite by a chelating ligand: An atomic force microscopy study. Geochimica et Cosmochimica Acta, 59, 4623–4632.
Rich, C.I. (1969) Suction apparatus for mounting clay specimens on ceramic tile for x-ray diffraction. Soil Science Society of America Proceedings, 33, 815–816.
Rufe, E. and Hochella, M.F., Jr. (1999) Quantitative assessment of reactive surface area of phlogopite dissolution during acid dissolution. Science, 285, 874–876.
Russ, J.C. (1995) The Image Processing Handbook, 2nd Ed., 674 p. CRC, London.
Schlegel, M.L., Manceau, A., Chateigner, D., and Charlet, L. (1999) Sorption of metal ions on clay minerals: I. Polarized EXAFS evidence for the adsorption of Co on the edges of hectorite particles. Journal of Colloid and Interface Science, 215, 140–158.
Schofield, R.D. and Samson, H.R. (1953) The deflocculation of kaolinite suspensions and the accompanying change over from positive to negative chloride adsorption. Clay Minerals Bulletin, 2, 45–51.
Sposito, G. (1984) The Surface Chemistry of Soils, 277 p. Oxford University Press, New York.
Sun, B.N. and Baronnet, A. (1989a) Hydrothermal growth of OH-phlogopite single crystals. I. Undoped growth medium. Journal of Crystal Growth, 96, 265–276.
——(1989b) Hydrothermal growth of OH-phlogopite single crystals. II. Role of Cr and Ti adsorption on crystal growth rates. Chemical Geology, 78, 301–314.
Teng, H.H., Dove, P.M., Orme, C.A., and De Yoreo, J.J.. (1998) Thermodynamics of Calcite Growth: Baseline for Understanding Biomineral Formation. Science, 282, 724–727.
Towle, S.N., Brown, G.E., Jr., and Parks, G.A. (1999a) Sorption of Co(II) on metal oxide surfaces: I. Identification of specific binding sites of Co(II) on (110) and (001) surfaces of TiO_2 (rutile) by Grazing-Incidence XAFS Spectroscopy. Journal of Colloid and Interface Science, 217, 299–311.
Towle, S.N., Bargar, J.R., Brown, G.E., Jr., and Parks, G.A. (1999b) Sorption of Co(II) on metal oxide surfaces: II. Identification of Co(II)(aq) adsorption sites on the (0001) and (1–102) surfaces of a-Al_2O_3 by Grazing-Incidence XAFS Spectroscopy. Journal of Colloid and Interface Science, 217, 312–321.
Turpault M.-P. and Trotignon L. (1994) The dissolution of biotite single crystals in dilute HNO_3 at 24°C: Evidence of an anisotropic corrosion process of micas in acidic solutions. Geochimica et Cosmochimica Acta, 58, 2761–2775.
van Santen, R.A. (1982) Chemical-bonding aspects of heterogeneous catalysis. II. Solid acids. Recueil, Journal of the Royal Netherlands Chemical Society, 101, 157–163.
Wehrli, B. (1989) Monte-Carlo simulations of surface morphologies during mineral dissolution. Journal of Colloid and Interface Science, 132, 230–242.
White, G.N. and Zelazny, L.W. (1988) Analysis and implications of the edge structure of dioctahedral phyllosilicates. Clays and Clay Minerals, 36, 141–146.
Wieland, E. and Stumm, W. (1992) Dissolution kinetics of kaolinite in acidic aqueous solutions at 25 °C. Geochimica et Cosmochimica Acta, 56, 3339–3355.
Wieland, E., Wehrli, B., and Stumm, W. (1988) The coordination chemistry of weathering. III. A generalization on the dissolution rates of minerals. Geochimica et Cosmochimica Acta, 52, 1969–1981.
Xiao, Y. and Lasaga, A.C. (1994) Ab initio quantum mechanical studies of the kinetics and mechanisms of silicate dissolution: H^+ (H_3O^+) catalysis. Geochimica et Cosmochimica Acta, 58, 5379–5400.
Zachara, J.M. and McKinley, J.P. (1993) Influence of hydrolysis on the sorption of metal cations by smectites: Importance of edge coordination reactions. Aquatic Sciences, 55, 250–261.
Ziolkowski, J. (1986) Crystallochemical model of active sites on oxide catalysts. Journal of Catalysis, 100, 45–58.
Zysset, M. and Schindler, P.W. (1996) The proton promoted dissolution kinetics of K-montmorillonite. Geochimica et Cosmochimica Acta, 60, 921–931.

MANUSCRIPT RECEIVED NOVEMBER 4, 1999
MANUSCRIPT ACCEPTED NOVEMBER 27, 2000
MANUSCRIPT HANDLED BY ALAIN BARONNET